Geochimica et Cosmochimica Acta 369 (2024) 213–226

Contents lists available at ScienceDirect

Geochimica et Cosmochimica Acta

journal homepage: www.elsevier.com/locate/gca

Lithium isotopes in water and regolith in a deep weathering profile reveal imbalances in Critical Zone fluxes

Di Cai [a,1,*], Michael J. Henehan [a,2], David Uhlig [b], Friedhelm von Blanckenburg [a,b]

[a] GFZ German Research Centre for Geosciences; Section 3.3 Earth Surface Geochemistry; Telegrafenberg, 14473 Potsdam, Germany
[b] Institut für Geologische Wissenschaften, Freie Universität Berlin, Malteser Str. 74-100, 12249 Berlin, Germany

ARTICLE INFO

Associate editor: Jiubin Chen

Keywords:
Lithium budget
Chemical weathering
Black Forest
Secondary mineral formation
Cation exchange
Hydrological budget
Groundwater

ABSTRACT

To trace Critical Zone processes and to quantify Li fluxes from one Critical Zone compartment into another, we investigated the Li concentration and isotopic composition (δ^7Li) of time-series water samples (including subsurface flow, groundwater and creek water), vegetation, bedrock (including separated minerals from bedrock), and regolith (including exchangeable fraction and clay-sized fraction of regolith) in a temperate forested headwater catchment in the Black Forest, Conventwald, Germany. Our estimation of the Li budget shows that atmospheric deposition and biological processes played minor roles in the Li cycle relative to chemical weathering. All water samples (δ^7Li value of 6.5 to 20.4 ‰) were enriched in ^{7}Li compared to bedrock (-1.3 ‰) and regolith (~-1.7 ‰), but δ^7Li differed between water pathways: δ^7Li variations in subsurface flow, creek water and groundwater were controlled by conservative mixing, exchangeable pool buffering and Li incorporation/adsorption, respectively. Fractionated heavy Li isotopes in water samples resulted from the formation of secondary solids which preferentially incorporated ^{6}Li, with the separated clay-sized fraction of the regolith exhibiting more negative δ^7Li values (-5.4 to −3.5 ‰) than the bulk regolith (~-1.7 ‰). However, Li in secondary solids only accounted for 8 ± 6 % of the total Li hosted in bulk regolith, and consequently δ^7Li in soil did not differ significantly from δ^7Li in bedrock. This is unexpected considering water is continuously removing ^{7}Li in preference over ^{6}Li from regolith. Mass balance calculations applied at the catchment scale point to an irreconcilable imbalance with our data. On one hand, the regolith's δ^7Li values are not negative enough to balance the ^{7}Li export by river water, and on the other hand Li in the riverine dissolved load only accounts for ~30 % of the Li solubilized from regolith. Therefore, we suggest that there might be a "hidden export pathway" for Li at our site, possibly subsurface removal of fine particles enriched in ^{6}Li. In light of increasingly frequent observations of such isotopic imbalances in the Critical Zone this phenomenon deserves increased attention.

1. Introduction

A key consideration of research in the Critical Zone - the thin layer of the Earth which extends from the top of the vegetation canopy down to deep aquifers (Brantley et al., 2007) - is mass transfer from one Critical Zone compartment (e.g., bedrock, soil, biota, or water) into another. Isotope ratios of metal(loid) elements have been suggested as a powerful tool to identify Critical Zone processes and to quantify relative fluxes of mass transfer in the Critical Zone (Bouchez et al., 2013; Sullivan et al., 2016; von Blanckenburg et al., 2021). Among these metal(loid) elements, lithium (Li) is mainly hosted in silicate minerals (Kısakűrek et al., 2005) and thought to be insensitive to biological processes (Lemarchand et al., 2010). As a result, the isotopic composition of Li has proven an ideal tracer for silicate chemical weathering (e.g. Huh et al., 1998; Pistiner and Henderson, 2003; Misra and Froelich, 2012; Dellinger et al., 2015). Isotope shifts of more than 70 ‰ have been observed among the Critical Zone compartments (Tomascak et al., 2016; Penniston-Dorland et al., 2017; Chapela Lara et al., 2022 and references therein) due to the large relative mass difference (~17 %) between ^{6}Li and ^{7}Li.

Following early work on the Li isotope composition of world rivers (Huh et al., 1998), numerous field studies and laboratory experiments have investigated the behaviour of Li isotopes during silicate

* Corresponding author.
E-mail address: dcai@tongji.edu.cn (D. Cai).
[1] Now at State Key Laboratory of Marine Geology, Tongji University, Shanghai, China.
[2] Now at School of Earth Sciences, University of Bristol, Queen's Road, Bristol, UK.

https://doi.org/10.1016/j.gca.2024.01.012
Received 6 May 2023; Accepted 13 January 2024
Available online 18 January 2024

weathering. These studies greatly deepened our understanding of Li isotope fractionation during the interaction between water, primary minerals, and secondary solids. Generally speaking, dissolution of Li isotopes from primary minerals is thought to be congruent, at least at conditions close to chemical equilibrium (Bouchez et al., 2013; Li et al., 2021; Zhang et al., 2021). During the formation of secondary solids and the adsorption of Li onto surfaces of oxides or clay minerals the light isotope ^{6}Li is favoured, which leads to a relative enrichment of heavy ^{7}Li in the remaining solution (e.g. Huh et al., 1998, 2001; Pogge von Strandmann et al., 2006, 2017; Vigier et al., 2009; Millot et al., 2010; Dellinger et al., 2015; Wang et al., 2015; Zhang et al., 2021). Consequently, the isotope composition of Li (^{7}Li/^{6}Li ratios expressed as δ^7Li values) of weathered material such as regolith is more negative than the δ^7Li value of parent bedrock. Correspondingly, the δ^7Li value of the fluid is more positive than the δ^7Li value of regolith (Penniston-Dorland et al., 2017 and references therein). The apparent isotope fractionation factors ($\Delta^7Li_{regolith\text{-}fluid}$) associated with these processes have been experimentally quantified in several studies (e.g. Vigier et al., 2008; Wimpenny et al., 2010a, 2015; Hindshaw et al., 2019; Li and Liu, 2020), with the magnitude of apparent isotope fractionation dependent on whether Li enters structural sites ($\Delta^7Li_{solid\text{-}solution} = \sim -18$ ‰ at room temperature; Vigier et al., 2008; Hindshaw et al., 2019) or exchangeable sites ($\Delta^7Li_{ex\text{-}solution}$ = -36 ‰ to ~ 0 ‰; Pistiner and Henderson, 2003; Wimpenny et al., 2015; Li and Liu, 2020,2022; Zhang et al., 2021) of secondary solids. With respect to the exchangeable site, the magnitude of isotope fractionation also depends on whether Li forms an outer-sphere exchangeable complex (little fractionation) or an inner-sphere exchangeable complex (large fractionation) (Hindshaw et al., 2019; Li and Liu, 2022).

Given the sensitivity of changes in the ^{7}Li/^{6}Li ratio during processes that incorporate Li into solids, the Li isotope system is a powerful tracer to explore geological and hydrological processes in the Critical Zone. From a mass balance perspective, it is now widely accepted that the riverine δ^7Li value is determined by the relative contribution of isotopically fractionated Li left behind in the fluid after Li incorporation into secondary solids, and Li congruently dissolved from primary minerals (e.g. Millot et al., 2010; Lemarchand et al., 2010; Pogge von Strandmann et al., 2012, 2017; Pogge von Strandmann and Henderson, 2015; Murphy et al., 2019; Chapela Lara et al., 2022). As Bouchez et al. (2013) inferred from an isotope model, congruent weathering of Li (with negligible secondary mineral formation fractionating δ^7Li) occurs in two endmember scenarios: 1) low denudation rate settings, where secondary minerals are re-dissolved; 2) high denudation rate settings, where Li-bearing secondary solids are not formed in sufficient amounts. The largest degree of Li isotope fractionation takes place at an intermediate weathering intensity. This conceptual framework has since been shown to be consistent with observations of dissolved Li in rivers integrating large catchments (Dellinger et al., 2015).

Within a catchment, however, large variations in δ^7Li values have been observed in time series of water samples (e.g. Liu et al., 2015; Henchiri et al., 2016; Zhang et al., 2022), suggesting that hydrological parameters control the isotope fractionation of Li beyond lithological and tectonic forces. One way to explain this variability is that heavy rainfall might alter flow paths and thus change Li sources. For instance, soil solutions in different depth of a single regolith profile can exhibit different Li fractionation regimes (Golla et al., 2021). Therefore, in response to varying hydrological conditions and fluid flow-path change, changing Li sources within the regolith can result in variation in the δ^7Li value of outlet runoff (Lemarchand et al., 2010; Henchiri et al., 2016; Fries et al., 2019). Factors such as the residence time of water, pH or temperature have also been suggested to influence δ^7Li values in a given catchment (Wanner et al., 2014; Liu et al., 2015; Gou et al., 2019; Zhang et al., 2022; Zhu et al., 2023).

Previous research generally focused on one compartment of the Critical Zone (e.g. weathering profile or river) and little has been done to simultaneously trace δ^7Li evolution of both dissolved and solid phases, and further, to reconcile the coupled evolution of these Li reservoirs. Key to transforming the complexity of Li isotope fractionation into a consistent framework of the partitioning of Li isotopes in the Critical Zone are surveys that explore all compartments in a watershed across different subsurface depths over time. This opportunity arose in a small, mono-lithological well-studied catchment (Conventwald, the Black Forest, Germany). This catchment has been (hydro-)geochemically characterized with respect to dissolved P (Sohrt et al., 2019), colloids (Gottselig et al., 2020) and Mg stable isotopes (Cai et al., 2022). Recently also, this site has played host to the development of the "organic nutrient cycle" and the "geogenic nutrient pathway" as novel concepts in Critical Zone research (Uhlig et al., 2020; Uhlig and von Blanckenburg, 2019a). Building on this body of work, we collected a time series of creek water, subsurface flow (0–15 cm depth) and groundwater samples to trace the δ^7Li value of dissolved Li through time. Seasonal patterns in these samples were investigated, along with measurements of bedrock, vegetation, bulk regolith, clay-sized fraction, and the exchangeable fraction of regolith. We aimed to decipher the driving forces of δ^7Li variations in both solid and dissolved phases and balance Li isotopes cycling from a catchment scale. Our measurements reveal diverse patterns of variability in each compartment: although water samples are all enriched in ^{7}Li compared to bedrock, time series of subsurface flow, groundwater and creek water show strongly divergent patterns. We evaluate the diverse causal drivers for these disparate trends in δ^7Li values in different compartments, adding another example (see also e.g. Golla et al., 2021) of how one Critical Zone site can comprise multiple distinct 'reactors' – often with very different fractionation regimes – that contribute very differently to the integrated catchment-scale dissolved Li budget. Critically, however, when viewed in the context of the whole catchment, the preferential export of ^{7}Li by water could not be balanced by the δ^7Li of the profile, as revealed by our mass balance model. We suggest therefore that a hidden export pathway – subsurface erosion – plays an important role at our site, and merits further consideration when investigating Critical Zone element cycling elsewhere.

2. Field setting

Samples were collected from a well-instrumented forest site "Conventwald" (48°02′0N, 7°96′0E), located in the Black Forest, southern Germany. This observatory is operated as part of the long-term forest ecosystem monitoring program "International Co-operative Program on assessment and monitoring of air pollution effects on forests (ICP Forest Level II)" and represents also one of the study sites of the DFG priority program SPP 1685 "Ecosystem Nutrition—Forest Strategies for limited Phosphorus Resources". The monitored creek catchment has an area of 0.077 km2 and the average elevation was ~ 840 m above sea level. Mean annual temperature at the study site is 6.8 C, and mean annual precipitation is 1395 mm/a. The underlying bedrock is paragneiss, which was developed from metamorphosed sedimentary rock in the Precambrian. Weathered bedrock was found at ~ 7 m depth and unweathered bedrock was encountered at ~ 16 m depth during a core-drilling campaign at the site (Uhlig and von Blanckenburg, 2019a). The soil type is classified as a hyperdystric skeletic folic Cambisol (WRB, 2014) with a loamy or sandy loamy texture and a mor-type moder forest floor atop. A detailed site description is provided by Lang et al., (2017). Although the study site was not glaciated during the Quaternary, periglacial slope deposits developed during the last glacial maximum. The uppermost metre of soil had a rock fragment content of ~70 %. The vegetation is mainly composed of European beech (*Fagus sylvatica*, ~40 %) and Norway spruce (*Picea abies*, ~45 %).

3. Methods

3.1. Sampling and sample terminology

The sampling strategy was presented in detail by Uhlig and von

Blanckenburg (2019a) for regolith samples and Sohrt et al. (2019) for water samples. Briefly, shallow regolith was sampled at depth increments of 20 cm in a 3 m deep trench. Deeper regolith beyond 3 m was retrieved using diesel-powered wireline core-drilling to ~ 20 m. For ease of reference, we distinguish between four layers in the weathering profile (Fig. 1): 1) the soil layer (strongly weathered, enriched in TOC and impacted by biota), 2) saprolite (which is weathered but retains the texture of underlying bedrock), 3) weathered rock (fractured with trace signs of alteration), and 4) fresh bedrock at depth. We use the term regolith to describe the weathering profile above the fresh bedrock, including soil, saprolite and weathered bedrock. 'Bulk regolith' is used to describe samples of untreated (only dried and sieved) regolith material retrieved from drill cores, differentiating from any extracted fractions (like clay-sized fraction or exchangeable fraction). We use the term 'secondary solids' to denote the secondary phases (like secondary clay, oxides and amorphous phases) neo-formed during chemical weathering processes, as opposed to remaining unaltered primary minerals inherited from bedrock (like feldspar and amphibole). Time-series water samples were collected from 01.03.2015 to 25.02.2016. Open rainfall and throughfall were collected bi-weekly in bulk containers covered by a netting mesh. Creek discharge was collected daily at midnight by an autosampler at a V-notched discharge weir. Groundwater was sampled daily by an autosampler from a well installed into the borehole after drilling. The groundwater table level was monitored by a pressure probe installed 10.9 m below the surface. Subsurface water from subsurface flow collectors installed at three depths in soil and subsoil (see Bachmain and Weiler 2012) was collected at the depth intervals 0–15 cm, 15–150 cm, and 150–320 cm. Due to limited availability of water samples from 15 to 150 cm and 150–320 cm, we only analysed the 0–15 cm subsurface flow samples for Li isotopes in this study. All water samples were acidified and stored at 4 °C before analysis. Living wood, beech leaves and spruce needles were collected from representative mature and young trees, and oven dried prior to further sample processing.

3.2. Extraction of the exchangeable fraction, separation of clay-sized fraction, and separation of primary minerals

Bulk regolith and bedrock samples were selected from representative depths and pulverized to < 60 µm (Uhlig and von Blanckenburg 2019a). For the extraction of the exchangeable fraction, soil and saprolite samples were first oven-dried and sieved to < 2 mm. 2 g of selected samples were accurately weighed and added to 15 ml acid-cleaned polypropylene centrifuge tubes pre-filled with 14 ml of a 1 M NH_4OAc solution. Samples were agitated, and the resulting suspensions shaken on a hotdog roller at 60 rpm for 3 h. After reaction, the suspensions were centrifuged at 4200 rpm for 30 min, before the supernatant was pipetted off into a syringe and filtered through a 0.2 µm acetate filter. Solutions were then split into two separate aliquots for major element concentration and Li isotope analysis. Afterwards, the NH_4OAc-extracted soil and saprolite samples were rinsed twice with deionised water (18.2 MΩ cm, TOC < 3 ng/g, Merck Millipore, Germany). The clay-sized fractions of these samples were then separated by centrifugation following the USGS method (Poppe et al., 2001). To evaluate the Li isotopic composition of individual minerals in bedrock, bedrock was first crushed and then sieved to 125 µm – 1 mm. The felsic minerals (mainly quartz and feldspar) were first removed using a magnetic separator. Hornblende, chlorite, and biotite were hand-picked under a microscope (Cai et al., 2022). Chlorite and biotite grains, formed from metamorphosed hornblende, generally contained relict traces of hornblende.

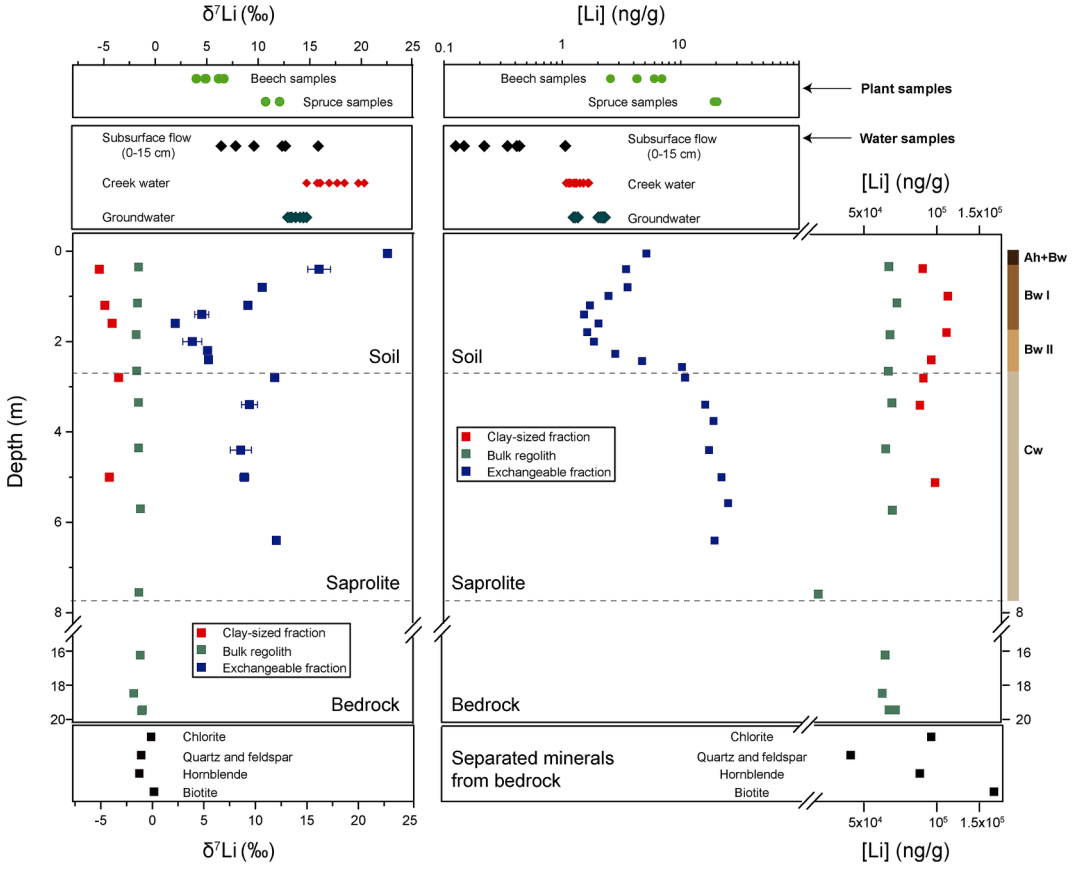

Fig. 1. δ^7Li values (left panel) and Li concentrations ([Li], right panel) of all Critical Zone compartments measured in this study. Uncertainty shown for the exchangeable fraction represents the twofold standard deviation of 3 replicate measurements. The uncertainty of the other samples is smaller than the symbol size. Ah, Bw, Cw: Soil horizons according to WRB, (2014).

3.3. Analytical methods

All measurements were performed in the Helmholtz Laboratory for the Geochemistry of the Earth Surface (HELGES) at GFZ Potsdam. Soil, saprolite, the extracted clay-sized fraction, primary minerals, and bedrock were dissolved by acid digestion using a mixture of concentrated HF and HNO_3 in PFA vials. *Aqua regia* was also applied to assist digestion after HF and HNO_3 treatment. Lithium concentrations of the filtered supernatant exchangeable fraction (Sec. 3.2 above), acidified water samples, and acid-digested solids (including minerals, bulk regolith, clay sized fraction and bedrock) were measured by quadrupole inductively coupled plasma mass spectrometry (Q-ICP-MS, iCAP, Thermo Fisher Scientific, Germany). The precision and accuracy of resulting concentration measurements were evaluated by replicate analyses of standard reference materials (SRM 2709a, BHVO-2, SLRS-6, SRM 1515, see Tables S1 to S4 in the data publication by Cai et al., 2021). Uncertainties on Li concentrations amount to about 8 % for most samples except for plant and water samples, which were analysed close to the limit of quantification of about 0.1 ng/g and thus have uncertainties of ~ 10 %. For Li isotope measurements, the digested solutions were dried and re-dissolved in 0.2 M HCl for cation exchange chromatography. 3.0 ml of Bio-Rad AG 50 W X12 200–400 mesh was loaded in BRAND 50 ml pipette PP columns (I.D. 6.4 mm, resin height 9.3 cm in deionised water). The matrix was eluted with 26 ml 0.2 M HCl and Li was collected in 23.5 ml 0.2 M HCl. The purified Li fractions were evaporated to dryness and re-dissolved in 1 ml of 0.3 M HNO_3. Purity and Li yield were assessed by Q-ICP-MS.

Lithium isotope ratios were measured on a multi collector inductively coupled plasma mass spectrometer (MC-ICP-MS, Neptune Plus, Thermo Fisher Scientific, Germany) equipped with a Jet Interface (Jet sample and X skimmer cones) and an ESI Apex Q desolvating introduction system. Instrumental mass bias was corrected via sample-standard bracketing against LSVEC lithium carbonate (Qi et al., 1997). An individual measurement consisted of 10 cycles of 4.2 s integration time, with ^{7}Li and ^{6}Li signals detected simultaneously in Faraday cups L4 and H4, equipped with 10^{11} Ω amplifiers. The typical signal intensity was ~ 0.5 V/ppb for ^{7}Li. Prior to analysis the Li concentration in the sample solutions were adjusted to match the bracketing standard solution concentration (20 ng/mL) to within 5 % in 0.2 M HNO_3. According to sample availability samples were measured two to four times during each session. For extracted exchangeable fractions and some water samples where the Li content was low, sample solutions and bracketing standard solutions were adjusted to ~ 2 ng/mL for isotope measurements. Background signals (<20 mV for ^{7}Li) were monitored with blank solutions (0.2 M HNO_3) and subtracted from sample signal intensities for both isotopes. Lithium isotope ratios are reported in the common delta notation relative to the reference material LSVEC: $\delta\ ^7Li\ (‰) = [(^7Li/^6Li)_{sample}/(^7Li/^6Li)_{LSVEC}\text{-}1] \times 1000$. The long-term internal reproducibility was gauged by measurement of LSVEC (0.1 ± 0.2 ‰, n = 28). SLRS-6 (river water, 24.0 ± 0.3 ‰, n = 5), SRM1515 (apple leaves, −1.0 ± 0.1 ‰, n = 2), OSIL (seawater, 30.9 ± 1.5 ‰, n = 3), SRM2709a (soil, −0.2 ± 0.1 ‰, n = 2) and BHVO-2 (basalt, 4.9 ± 0.7 ‰, n = 3) were routinely monitored to gauge the external reproducibility (see Tables S1 to S4 in the data publication by Cai et al., 2021).

3.4. Li transfer rates and fluxes among different Critical Zone compartments

To derive the rates of Li input and output in the Critical Zone at Conventwald (Table 1) we make use of previously published fluxes calculated by Uhlig and von Blanckenburg (2019a) that are based on data available in an open access data publication (Uhlig and von Blanckenburg 2019b). We combined these with Li concentration measurements from the present study. The denudation rate D was measured with *in situ* cosmogenic ^{10}Be in quartz sediment at the outlet of the catchment and equated to the soil production rate RP (Uhlig and von

Table 1
Glossary of metrics used in this study.

Name	Description	Calculation		Explanation
Li inventories (in g/m^2)				
I^{Li}_{bulk}	Inventory of Li in bulk regolith	$I^{Li}_{bulk} = \int_0^z [Li_{bulk}]_z \times \rho \times dz$	(1)	z is the depth of the weathering profile and ρ is the density of bulk regolith. $[Li_{bulk}]_z$ is the Li concentration of bulk regolith at depth z.
I^{Li}_{ex}	Inventory of Li in the exchangeable fraction of regolith	$I^{Li}_{ex} = \int_0^z [Li_{ex}]_z \times \rho \times dz$	(2)	z is the depth of the weathering profile and ρ is the density of bulk regolith. $[Li_{ex}]_z$ is the Li concentration of the exchangeable fraction in regolith at depth z.
Li rates and fluxes (in g/m^2/ yr)				
D	Denudation rate			Denudation rate is estimated from cosmogenic nuclides (Uhlig and von Blanckenburg, 2019a).
D^{Li}	Denudation rate of Li	$D^{Li} = D \times [Li]_{bedrock}$	(3)	$[Li]_{bedrock}$ is the Li concentration in bedrock.
RP^{Li}	Regolith production rate of Li	$RP^{Li} = D^{Li}$	(4)	At steady state, the regolith production rate is identical to the denudation rate.
$W^{Li}_{regolith}$	Regolith weatheringrate of Li	$W^{Li}_{regolith} = D \times [Li]_{bedrock} \times (-\tau^{Li})$	(5)	Net solubilisation flux of Li from regolith. See eq. (10) for calculation of τ^{Li}.
W^{Li}_{river}	River weathering rate of Li	$W^{Li}_{river} = \sum_{i=1}^{365} \frac{[Li]_i \times Q_i}{A}$	(6)	Annual dissolved Li weathering flux, which is the sum of catchment area (A) normalized products of daily river Li concentration [Li] and daily discharge (Q) of a hydrological year.
$E^{Li}_{regolith}$	Regolith erosionrate of Li	$E^{Li}_{regolith} = D \times [Li]_{bedrock} \times (1 + -\tau^{Li})$	(7)	Erosion rate of Li from regolith.$E^{Li}_{Regolith} + W^{Li}_{Regolith} = D^{Li}$
U^{Li}	Plant uptake rate of Li	$U^{Li} = \frac{NPP \times [Li]_{tree}}{[C]_{tree}}$	(8)	$[C]_{tree}$ denotes carbon concentration in dry mass (~50 %). NPP means net primary productivity, which is approximately half of GPP (gross primary production).

(*continued on next page*)

Table 1 (*continued*)

Name	Description	Calculation		Explanation
Dep^{Li}_{wet}	Wet deposition of Li	$Dep^{Li}_{wet} = [Li]_{precipitation} \times F_{precipitation}$	(9)	$F_{precipitation}$ denotes annual flux of precipitation and $[Li]_{precipitation}$ means Li concentration in precipitation.
Li mass fractions and flux ratios (dimensionless)				
τ^{Li}	Elemental mass transfer coefficient	$\tau^{Li} = \frac{[Li]_{regolith}}{[Zr]_{regolith}} \times \frac{[Zr]_{bedrock}}{[Li]_{bedrock}} - 1$	(10)	Fractional mass loss or gain of an element relative to bedrock, where negative τ^{Li} denotesloss of Li.
f^{Li}_{sec}	Fraction of Li in secondary solids	$f^{Li}_{sec} = \frac{\delta^7 Li_{soil} - \delta^7 Li_{bedrock}}{\delta^7 Li_{secondary} - \delta^7 Li_{bedrock}}$	(11)	Fraction of Li carried by secondary solids relative to total soil Li calculated by end-member mixing model
$w^{Li}_{isotope}$		$w^{Li}_{isotope} = \frac{\delta^7 Li_{soil} - \delta^7 Li_{rock}}{\delta^7 Li_{soil} - \delta^7 Li_{water}}$	(12)	Ratio of Li exported in the dissolved phase calculated from isotope ratios expressed as delta values (Bouchez et al., 2013)
DEE^{Li}	Dissolved export efficiency of Li	$DEE^{Li} = \frac{W^{Li}_{river}}{W^{Li}_{regolith}}$	(13)	Ratio of the flux of Li found in dissolved river export (W^{Li}_{river}) relative to the flux of Li released by weathering in regolith ($W^{Li}_{regolith}$).
DEE^{Li}_{Na}	Na-normalised dissolved export efficiency of Li	$DEE^{Li}_{Na} = \frac{W^{Li}_{river}/W^{Na}_{river}}{W^{Li}_{regolith}/W^{Na}_{regolith}} = \frac{(\frac{[Li]}{[Na]})_{river}/(\frac{[Li]}{[Na]})_{bedrock}}{\tau^{Li}_{Zr}/\tau^{Na}_{Zr}}$	(14)	DEE is normalised by the conservative element Na so that the ratio is independent of rate estimates and minimises dilution effects.

Blanckenburg, 2019a). Weathering rates and τ values made use of Zr concentrations in bedrock and regolith. Plant uptake of Li was calculated from net primary productivity (Uhlig and von Blanckenburg, 2019a). Throughfall and creek water discharge was presented by Sohrt et al. (2019).

4. Results

4.1. δ ^{7}Li values and [Li] of Critical Zone compartments

All data determined for this study and a previous study on Mg stable isotopes on the same samples Cai et al., (2022) is presented in a data publication that is available open access (Cai et al., 2021). Unweathered paragneiss bedrock yielded a δ^7Li value of ~ -1.3 ‰ (Fig. 1, Table S1). Of the separated minerals, amphibole (-1.3 ‰) and chlorite (-1.4 ‰) are isotopically similar to bulk bedrock (Fig. 1), whereas biotite (-0.7 ‰) and felsic minerals (-0.1 ‰) were isotopically slightly heavier than bulk bedrock (Fig. 1). δ^7Li values of bulk regolith were almost indistinguishable from bedrock and showed negligible variation throughout the weathering profile. The clay-sized fraction was relatively enriched in ^{6}Li with δ^7Li values ranging from −3.5 to −5.4 ‰ (Fig. 1, Table S1). In contrast, the exchangeable fraction represented not only the isotopically heaviest compartment in the regolith but also showed a systematic variation with depth. Specifically, the most positive δ^7Li value of 22.5 ‰ was found in the topsoil, followed by a gradual decrease from the surface to ~ 1.6 m depth to minimum values of 2.5 ‰, and a shift towards more positive δ^7Li values of about 11.6 ‰ at ~ 3 m depth. Below ~ 3 m depth δ^7Li values were largely invariable. Similar trends were found for the Li concentration of the exchangeable fraction (Fig. 1, Table S4). Beech leaves and twigs had Li concentrations ranging from 2 to 7 ng/g and similar δ^7Li values (5.5 ± 1.9 ‰, n = 6) (Figs. 1, 2, Table S3). Spruce needles had both higher Li concentrations (~20 ng/g) and more positive δ^7Li values (11.4 ‰, n = 2) than beech samples (Figs. 1, 2, Table S3).

4.2. Time series of [Li] and δ ^{7}Li values in water samples

Throughfall was very diluted in [Li] (3.3 nmol/l) and had a δ^7Li value of 8.4 ‰ (Table S2). This isotopic composition is indicative of a mixture of rainwater containing Li from sea spray (assumed to be similar to seawater, ~31 ‰, Hoefs, 2021) and the dissolution of Sahara dust inputs (δ^7Li = -0.7 ‰, Clergue et al., 2015) that may have occurred in summer 2015 (https://www.dwd.de). [Li] of subsurface flow (0—15 cm) ranged from 18 to 153 nmol/l (Fig. 3a, Table S2). δ^7Li values of subsurface flow (0–15 cm) showed the largest variation among the Critical Zone compartments of this study, ranging from 6.5 to 15.9 ‰ (Fig. 3a, Table S2). [Li] of groundwater was much higher than in subsurface flow, ranging from 180 to 331 nmol/l (Fig. 3b, Table S2). Although there was considerable variability in the [Li] of groundwater, its isotopic composition remained almost invariant throughout a hydrological year (13.9 ± 1.2 ‰, n = 9; Fig. 3b, Table S2). [Li] of creek water was similar to groundwater, ranging from 157 to 242 nmol/l (Fig. 3c, Table S2), while its δ^7Li values were similar to or more positive than groundwater, ranging from 14.8 to 20.4 ‰ (Fig. 3c, Table S2).

4.3. Summary of fluxes and inventories

Prior to discussing the evolution of the Li isotope composition in the Critical Zone, we first present an evaluation of the influence of wet deposition and plant uptake on the catchment's Li budget. For this purpose, we provide a glossary of all metrics and equations used for the calculation of metrics in this study with Table 1, which was introduced in detail in von Blanckenburg et al. (2021) and references therein. Fig. 4 shows the estimated budget of Li in the Critical Zone. The chemical weathering flux of Li ($W^{Li}_{regolith}$, eq. 5, Table 1) is ~ 460 times higher than the wet deposition flux of Li (Dep^{Li}_{wet}, eq. 9, Table 1). Thus, we suggest

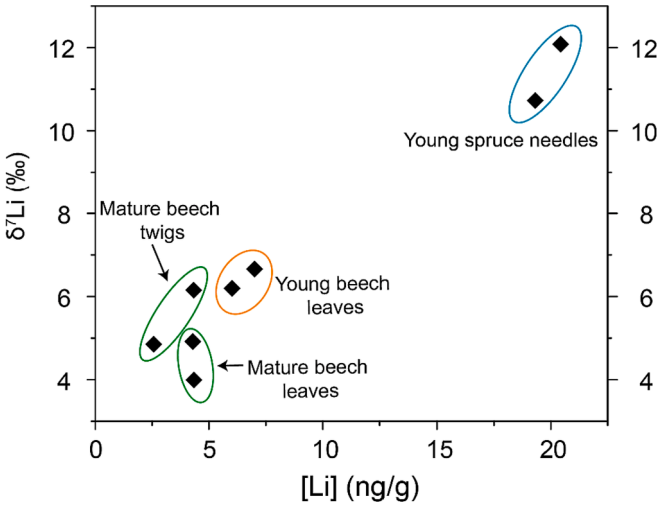

Fig. 2. Li concentration [Li] and isotope composition (δ^7Li) of plant samples. Mature beech twigs and leaves samples are from the same tree. Uncertainties are smaller than the symbol size.

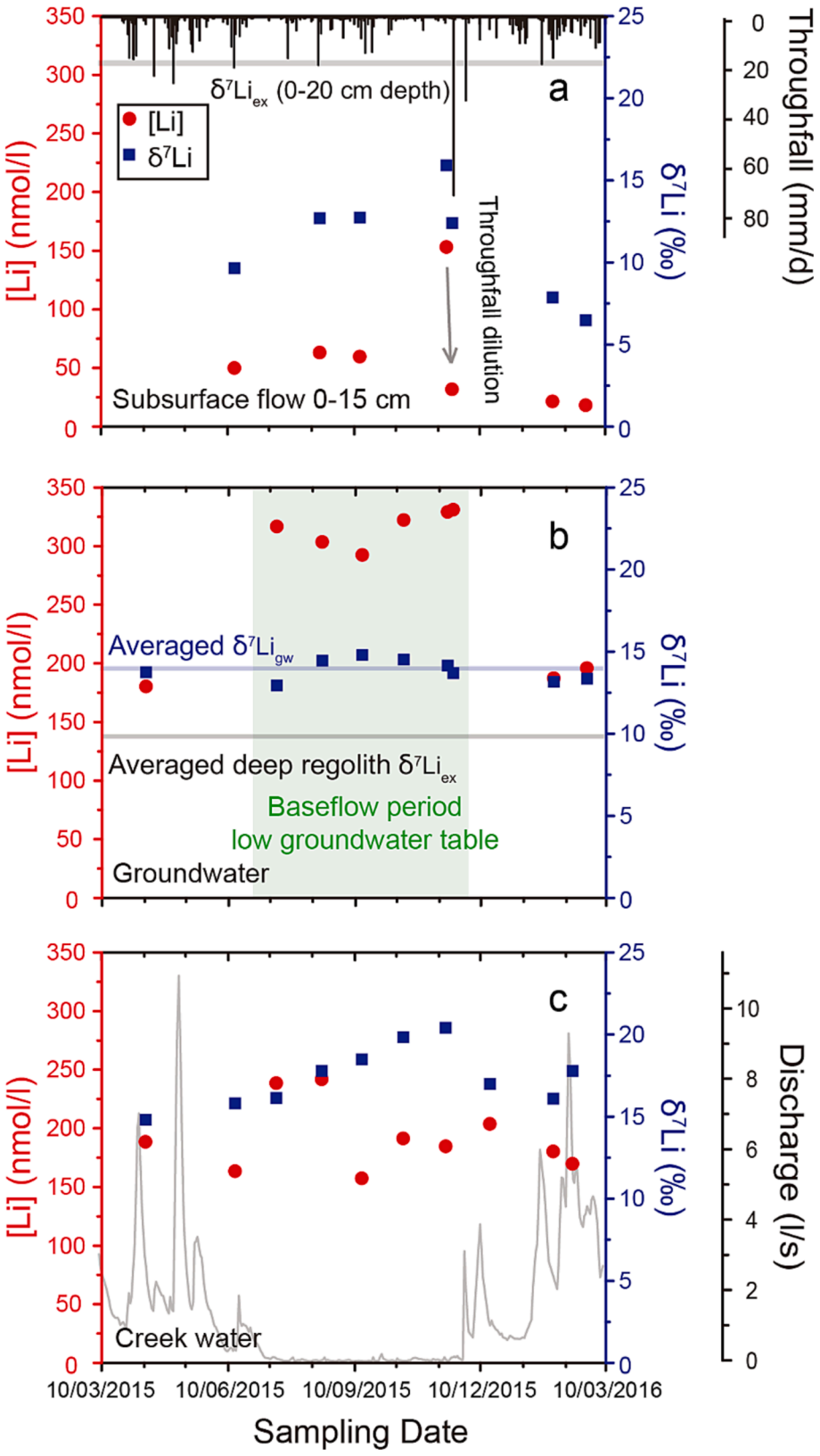

Fig. 3. Li concentration [Li] and Li isotope composition (δ^7Li) of time series water samples. Throughfall and creek water discharge (sourced from Sohrt et al., 2019) are also shown in panel a and c. Horizontal lines in panel a and b show the δ^7Li value of the exchangeable fraction at the corresponding depth. Uncertainties are smaller than the symbol size.

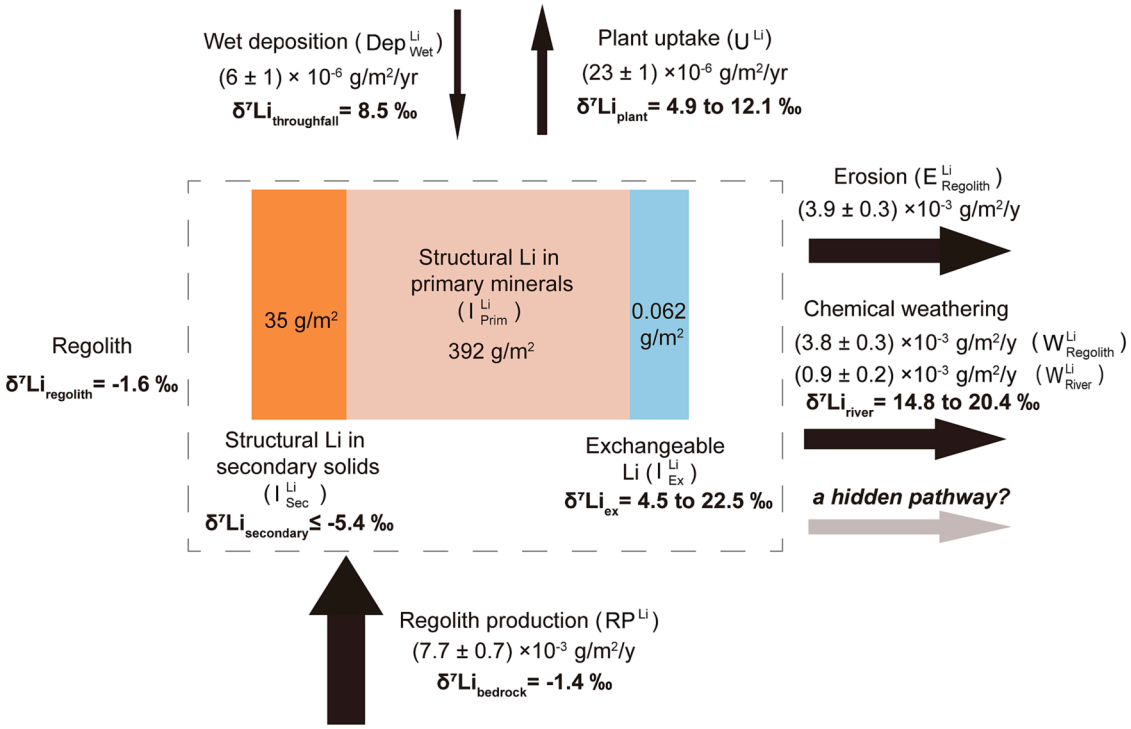

Fig. 4. Input-output fluxes and inventories of Li at the Conventwald. Arrow width corresponds to the flux magnitude. For the estimation of fluxes and inventories see Table 1.

that the contribution of wet deposition to the runoff of Li at this site is negligible. The biological influence on the Li budget of a catchment is generally thought to be minor, as Li is regarded to be a non-essential element for plants and its concentration in plant tissues is low (Lemarchand et al., 2010; Clergue et al., 2015). The plant uptake flux of Li (U^{Li}_{total}, eq. 8, Table 1) amounts to only 1 % of the chemical weathering flux, which confirms its likely negligible influence on the catchment Li budget and the Li isotope composition.

4.4. Weathering regime

Lithium concentrations of bulk regolith (Table S1) were converted to the mass transfer coefficient (τ^{Li}_{Zr}, Eq. 10 in Table 1, Brimhall and Dietrich, 1987). In doing so, Zr was used as reference element as justified in Uhlig and von Blanckenburg (2019a) and Zr concentrations were sourced from Uhlig and von Blanckenburg (2019b). τ^{Li}_{Zr} amounts to ~ -0.50 suggesting that ~ 50 % of Li was lost in soil and saprolite (Fig. 5).

5. Discussion

5.1. Li isotopic fractionation during pedogenesis

The Li isotopic composition of regolith is commonly thought to be set by any of three processes: 1) atmospheric input (e.g., Liu et al., 2013; Clergue et al., 2015); 2) preferential dissolution of more weatherable minerals (e.g., Zhang et al., 2021); or 3) secondary mineral formation (e.g., Ryu et al., 2014; Pogge von Strandmann et al., 2021). However, at the Conventwald, we find virtually no vertical variation in δ^7Li values in regolith, and δ^7Li values are indistinguishable from those of parent rock, despite a Li loss of ~ 50 %. Concerning 1), dust input should be negligible at our site, as no enrichment of elements was observed in the shallow depth of the regolith. Furthermore, deep (~6 m) and shallow regolith samples feature almost identical mineralogical and geochemical characteristics (Uhlig and von Blanckenburg 2019a). As for 2), preferential dissolution of minerals, X-ray diffraction analysis (Uhlig and von

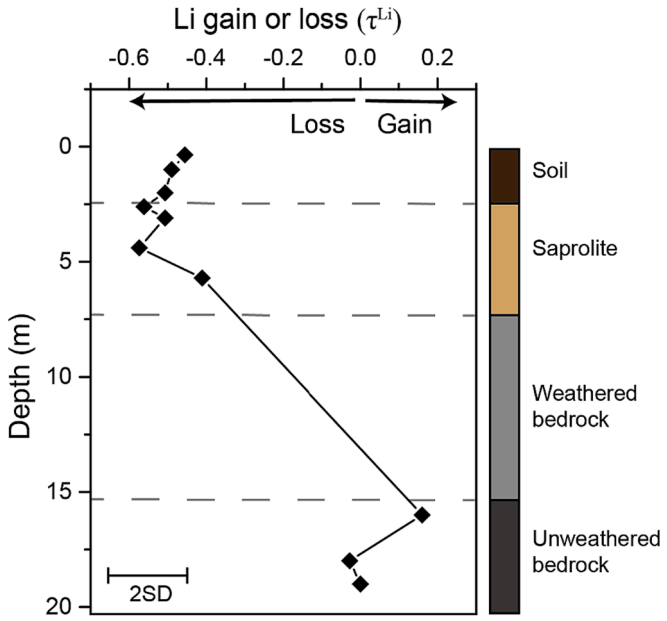

Fig. 5. Gain or loss of Li (τ^{Li}_{Zr}) throughout the weathering profile. Error bar represents two standard deviations (2SD) of the error-propagated external analytical uncertainty of Zr (±9 %, Uhlig and von Blanckenburg 2019b) and Li (±5 %, Cai et al., 2021) and amounts to 24 %.

Blanckenburg, 2019a) and Mg isotope measurements on these same samples (Cai et al., 2022) have revealed the preferential dissolution of hornblende in the regolith. However, we find Li isotopic compositions to be relatively uniform between different primary minerals (Fig. 1), and so preferential dissolution should not induce a large shift in Li isotope ratios. Concerning explanation 3), the clay-sized fraction separated from bulk soil and saprolite indeed exhibits higher Li concentrations and

more negative δ^7Li values (~-4 ‰) than the bulk regolith (Fig. 1). This observation is compatible with the formation of secondary minerals that preferentially incorporate ^{6}Li. However, a quantitative evaluation (Eq. 11) of relative Li fluxes into secondary solids presented in section 5.4 shows that this effect amounts to only 8 ± 6 % of the solid regolith's Li (see 5.4 for detailed discussion), which generates too small a shift to be detectable in bulk samples. One scenario to resolve this discrepancy might be that in the geologic past Li was dissolved and wholesale exported in the dissolved form (no secondary solids were formed), entailing no isotope fractionation, and that such weathering regime has since transited to one involving clay formation today. While theoretically possible, thorough examination of published data in river water consistently reveals higher δ^7Li values compared to those of the bedrock, and we have not encountered any documented case study that demonstrates chemical weathering without simultaneous shift in the Li isotope composition between bedrock and fluid. Therefore, below we alternatively suggest that indeed a certain amount of secondary minerals, characterized by fractionated Li isotopes, were formed, but that these were removed by a still undisclosed pathway likely involving the subsurface process. This process will be quantified and thoroughly discussed in section 5.4.

5.2. Controlling factors of [Li] and δ^7Li values of water samples

The subsurface flow water samples (0–15 cm) exhibit large variations in [Li] and δ^7Li values. Previous studies from Turton et al., (1992) and Zhao et al., (2013) have shown that the generation of subsurface water involves a mixing process of event water (i.e., throughfall) with pre-event water (i.e., soil water). Due to the shallow depth, the chemistry of subsurface flow should respond rapidly to rainfall input. Indeed, the subsurface flow water sample collected on the Nov. 20th 2015 was significantly diluted due to heavy throughfall that day (note the arrow in Fig. 3a, which indicates this dilution). Moreover, concentrations of Li and Cl (Cl is considered as a conservative element) decreased by three times compared to the sample collected 4 days earlier. The δ^7Li value of this sample also became more negative, approaching the δ^7Li value of throughfall. Moreover, water samples collected in different seasons show linear relationships in binary plots of Li vs. Cl and 1/Li vs. δ^7Li (Fig. 6a, b), confirming a two-endmember mixing process controlling the chemical composition of subsurface flow water. The throughfall

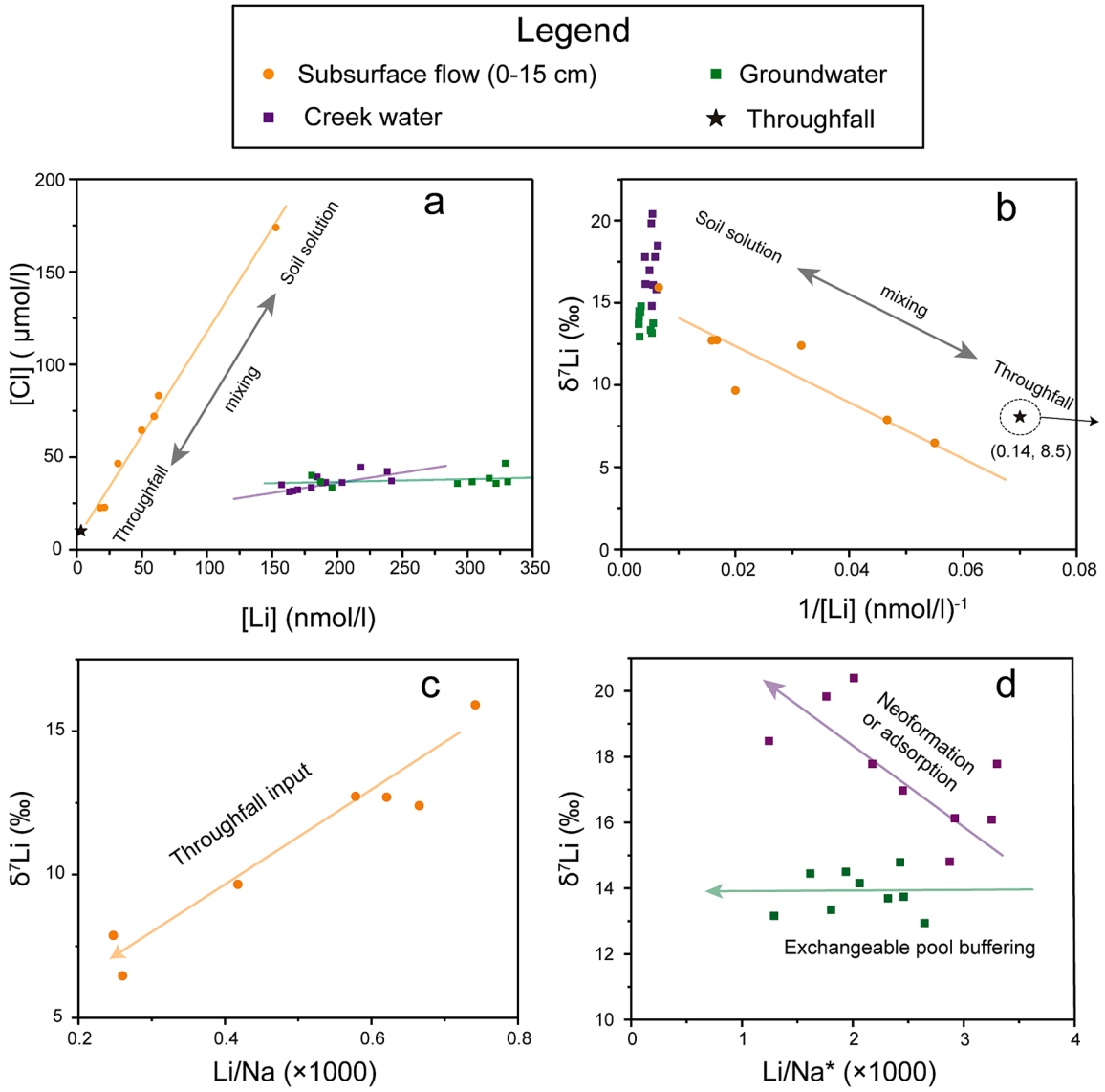

Fig. 6. Binary plots of a) [Li] vs. [Cl], b) [Li] vs. δ^7Li, c) Li/Na (the proportion of Li remaining in solution after formation of secondary minerals) vs. δ^7Li of subsurface flow and d) Li/Na* vs. δ^7Li of groundwater and creek water, Na* denotes that the Na content was corrected for atmospheric input. Cl is regarded as a conservative element here. Arrows illustrate processes. Uncertainties are smaller than the symbol size.

endmember is diluted in [Li] and [Cl] and depleted in ^{7}Li (Fig. 6a, b). Although not sampled in this study, pre-event water (soil solution) is expected to be concentrated in Li and Cl, and ^{7}Li, as inferred from the mixing line (Fig. 6a, b). These higher concentrations at shallow depth are likely due to evapotranspiration effects (Zhao et al., 2013). To exclude the possibility that shifts in δ^{7}Li values and [Li] are due to incorporation of Li into or adsorption of Li onto secondary phases we follow the approach from Millot et al., (2020) and Dellinger et al., (2015) by calculating the proportion of Li remaining in solution after secondary mineral formation (Li/Na) and plotting it against the δ^{7}Li value.

It is assumed that the initial ratio of $(Li/Na)_{water}$ is identical to that of bedrock and that Na is not incorporated into secondary phases (Gislason et al., 1996). If Li is incorporated into secondary minerals (i.e. low Li/Na), δ^{7}Li values in the dissolved load would increase. A negative trend in Li/Na vs. δ^{7}Li is generally observed in riverine water (e.g., Dellinger et al., 2015; Pogge von Strandmann et al., 2017; Murphy et al., 2019). However, for the 0–15 cm subsurface flow samples, a positive relationship between Li/Na and δ^{7}Li emerges (Fig. 6c). Therefore, we suggest that mixing with throughflow input, rather than any reaction process, directly controls both concentration and isotope composition of Li in shallow subsurface flow water. The binary mixing model for subsurface flow (0–15 cm) samples would predict that endmember soil solution at 0–15 cm depth should exhibit δ^{7}Li values > 16 ‰, consistent with secondary mineral formation in the regolith preferentially incorporating ^{6}Li.

Groundwater is characterized by longer fluid-regolith interaction times than shallow subsurface flow. If the fluid length scale is sufficiently long, groundwater solutes reach thermodynamic equilibrium with reacting solids (Maher, 2010; 2011). In this study site, groundwater has a much higher Li content compared to shallow subsurface flow, and low and uniform Cl concentrations. Consequently, Li/Cl ratios in groundwater do not follow the trend found in subsurface water (Fig. 6a). A dilution effect induced by groundwater recharge was found as the Li concentration decreased with the rise of the groundwater table (Fig. 7). However, when the level of the groundwater table increased from 8.4 m below ground to 6.4 m below ground, the Li concentration decreased only slightly from 187 nmol/L to 180 nmol/L suggesting that a buffering effect prevents [Li] in groundwater from decreasing below 180 nmol/L. More surprisingly, groundwater remained almost homogenous in δ^{7}Li values at ~ 13.9 ‰ through the hydrological year despite large changes in the Li concentration. Consequently, an unusual horizontal relationship between Li/Na* (Na* denotes atmospheric input-corrected Na concentration, assuming Cl is conservative and using Na/Cl in throughfall and groundwater for correction) and the δ^{7}Li value was observed (Fig. 6c). The buffering effect of [Li] could not be attributed to mineral dissolution since the dissolution process would drive δ^{7}Li values lower (approaching to the δ^{7}Li value of bedrock). To explain the invariance of δ^{7}Li values accompanied by buffered [Li], we adopted the interpretation of Kim et al., (2014) and that of our former study (Cai et al., 2022) who both proposed that there are two processes operating at different timescales, which regulate groundwater geochemistry: thermodynamic equilibrium of mineral dissolution-neoformation and a buffering effect by the exchangeable pool. We propose that in the baseflow period (from Jun. 10th 2015 to Oct. 10th 2015, Fig. 3b, 7), the groundwater table is low and it has sufficiently long reaction time so that thermodynamic equilibrium was attained, [Li] reached its maximum value (Maher, 2011) and Li isotopes were fractionated due to the competition between mineral dissolution and secondary mineral formation. Indeed, the Li isotopic composition shows a minute anti-correlation with [Li] during the baseflow period (Fig. 3b), and groundwater samples exhibiting slightly higher δ^{7}Li values with lower [Li] may reflect Li incorporation into secondary minerals. During the high flow period, when the groundwater table is high, infiltrated water recharging the groundwater aquifer may have shorter residence times and the exchangeable fraction rapidly buffered the water chemistry, while thermodynamic equilibrium with minerals was not attained. This mechanism was responsible for lower [Li] in groundwater (as in Kim et al., 2014). In both cases, Li isotope fractionation equilibrium was reached between the dissolved and the exchangeable phase, which results in the insignificant variance of δ^{7}Li values in groundwater throughout a hydrological year. The apparent Li isotope fractionation factor between groundwater and the regolith exchangeable pool ($\Delta^{7}Li_{gw\text{-}ex}$) is ~ 4 ‰ (Fig. 7), a value consistent with exchange experiments using smectite as adsorbent (~5 ‰, Li and Liu, 2022). It is noteworthy that the exchange direction might differ in different hydrological seasons. Concentrated groundwater during the baseflow period might have set the elemental and isotopic composition of the exchangeable fraction,

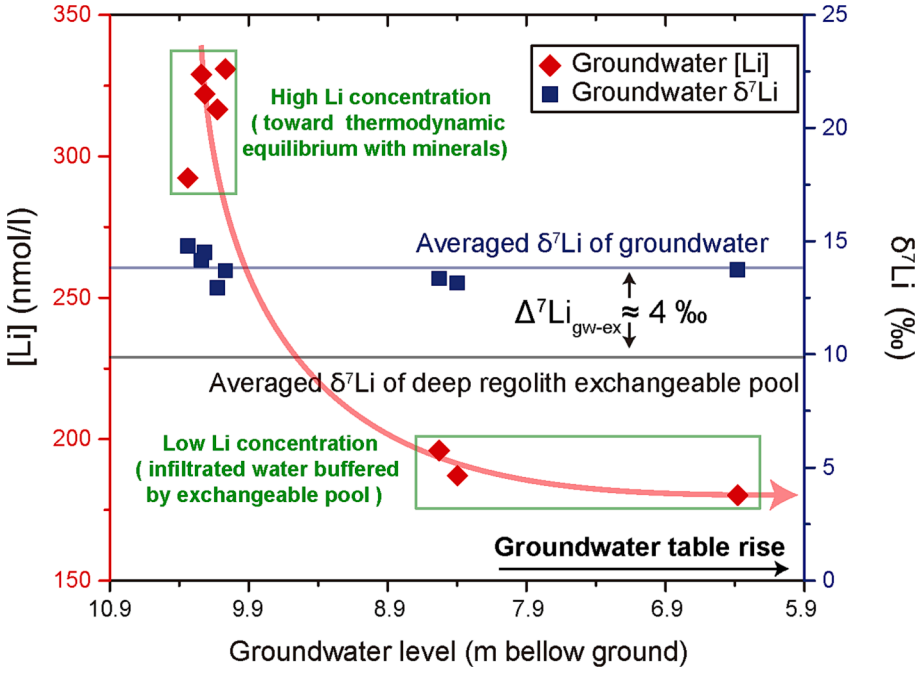

Fig. 7. Variation of Li concentration [Li] and isotope composition (δ^{7}Li value) of groundwater in response to groundwater level change.

and the exchangeable fraction in turn buffered infiltrated water during the high flow period. The same hypothesis was also proposed in our former study on Mg isotopes at Conventwald (Cai et al., 2022).

In creek water, Li/Cl relationships are more akin to groundwater than to subsurface flow (Fig. 6). δ ^{7}Li values of creek water (14.8 to 20.4 ‰) are similar to, or more positive than, groundwater samples (~13.9 ‰). Endmember mixing analysis (EMMA) at Conventwald has indicated that groundwater is the major source feeding creek water (Sohrt et al., 2019). The higher δ^{7}Li values in creek water than in groundwater may be caused by the ongoing formation of secondary solids or adsorption in the creek channel. Fig. 6c confirms this hypothesis as δ^{7}Li values of creek water increase with decreasing Li/Na* (Na* denotes atmospheric input corrected Na). This finding is consistent with worldwide trends in river water (e.g. Liu et al., 2015; Dellinger et al., 2015; Pogge von Strandmann et al., 2017). An increasing trend in δ^{7}Li values is observed during dry periods (Fig. 3c) and a negative correlation between discharge and δ^{7}Li is seen (Fig. 8), which might reflect more fractionated Li with increasing water residence time as water has more time to interact with solid phases (Liu et al., 2015; Zhang et al., 2022).

In summary, our study has identified three different pathways (mixing, exchangeable pool buffering and Li incorporation/adsorption) for dissolved δ^{7}Li evolution, implying that critical zone of different structures and hydrological conditions may see different evolution regimes in riverine δ^{7}Li. While both mixing (Henchiri et al., 2016) and Li incorporation (Liu et al., 2015) have already been invoked as direct driving forces of riverine δ^{7}Li variation, the buffering effect of the exchangeable pool has not been demonstrated before. It has been noted that the middle Yellow River shows a wide range in W/D (weathering rate/denudation rate) but a relatively constant δ^{7}Li (Gou et al., 2019; Pogge von Strandmann et al., 2020), deviating from the "boomerang" type relationship which predicts larger δ^{7}Li in intermediate W/D (Dellinger et al., 2015). We suggest that this unusual invariance of δ^{7}Li might reflect the effect of exchangeable pool buffering, given the high exchange capacity of Yellow River sediments (Tipper et al., 2021), or that denudation and export fluxes are not at steady state in the Yellow River (Gaillardet et al., 1999), potentially invalidating the relationship between W/D and δ^{7}Li.

5.3. *δ^{7}Li of regolith exchangeable fraction and isotope fractionation between exchangeable Li and dissolved Li*

The weakly-bound exchangeable fraction of regolith is sometimes regarded as an alternative record of the isotope composition of soil solution (e.g., Bullen and Chadwick, 2016; Li and Liu, 2020). It reflects a combined effect of primary mineral dissolution, secondary mineral formation, and bioactivity (Bullen and Chadwick, 2016; Cai et al., 2022). Our previous Conventwald study on Mg isotopes (Cai et al., 2022) has indicated that there is a negligible effect of Mg isotope fractionation during sorption processes, and that the Mg isotopic composition of groundwater and creek water have almost the same Mg isotopic composition as the deep regolith exchangeable pool. To evaluate whether this is the case for Li too, we compared δ^{7}Li values of the dissolved load with δ^{7}Li values of the corresponding exchangeable fraction. Deep groundwater (collected at ~ 10.5 m depth) exhibited almost invariant δ^{7}Li values. The corresponding deep regolith (>3 m) exchangeable fraction also shows small variations in δ^{7}Li values (Fig. 1). The apparent isotope fractionation factor between the deep exchangeable pool and deep groundwater $\Delta^7Li_{groundwater\text{-}exchangeable}$ is ~ 4 ‰ (Fig. 7). X-ray diffraction analysis at this site has identified chlorite and biotite as main phyllosilicates (Uhlig and von Blanckenburg, 2019a), and we suspect that these minerals constitute the main hosts for exchangeable cations (Cai et al., 2022). We suggest that our groundwater and exchangeable fraction are in equilibrium in terms of Li isotopic composition and associated fractionation is ~ 4 ‰ between the dissolved and adsorbed pools (section 5.2). This contrasts with subsurface flow (0–15 cm), where a large variability in δ^{7}Li values (6.5 to 15.9 ‰) can be explained by conservative mixing alone. We suggest this may be a function of kinetics, with flushing of subsurface flow being too fast for exchange reactions to manifest significant shifts in the fluid's isotope ratio.

Previous investigations of exchangeable Li and its isotopic composition in the Critical Zone are sparse (Li et al., 2020; Chapela Lara et al., 2022), and experimental studies on Li adsorption onto different geological matrices have shown highly variable isotope fractionation factors (e.g., Pistiner and Henderson, 2003; Hindshaw et al., 2019; Pogge von Strandmann et al., 2019; Li and Liu, 2020; Zhang et al., 2021) with exchangeable Li being isotopically more negative than Li in the dissolved load, as observed in this study. It is striking, then, that the exchangeable pool of the uppermost soil sample has a δ^{7}Li value of 22.5 ‰ – higher than all other samples analyzed (including throughfall and subsurface flow). Soil solution at this depth, although unsampled, is inferred from the mixing trend shown in Fig. 6b to have a δ^{7}Li value of ~ 18 ‰, a value still lower than 22.5 ‰. A potential explanation for this discrepancy might be that the extraction procedure that we used was incomplete, and hence isotope fractionation occurred. This has been observed in Li desorption experiments, where ^{7}Li was preferentially desorbed when the pH of reacting solution lowered from 8.5 to 4.3 (Li and Liu, 2020).

Nevertheless, the exchangeable fraction is always isotopically heavier than bulk regolith. We suggest that this is because secondary mineral formation favours ^{6}Li, driving δ^{7}Li in soil solution to be more positive, and hence the corresponding exchangeable fraction inherits this heavy isotopic composition signal. It is also noteworthy that both concentration and isotope composition of Li in the exchangeable fraction exhibit their lowest values at ~ 1.8 m, as Mg does (Cai et al., 2022). Although previous research indicates pH may influence δ^{7}Li fractionation during adsorption or secondary mineral formation (Li and Liu, 2020; Zhang et al.,2021; Zhu et al., 2023), the variation of δ^{7}Li of exchangeable fraction does not align with pH change here. Alternatively, for Mg, the "bulge shape" was attributed to a bio-uplift effect, meaning that vegetation takes up Mg at greater depth (favouring heavy Mg isotopes) and returned it to shallow depth via litterfall. This process results in both lower concentrations and more negative δ^{26}Mg values in the exchangeable fraction in the middle part of the soil column. Although Li is a non-nutritive element, this might be applicable for Li too (Fig. 9). The ratio of the Li uptake flux of plants (U^{Li}_{total}, Fig. 5) and the inventory of Li in the exchangeable fraction (I^{Li}_{ex}, Fig. 5) is proportionally half as high as for the macronutrient Mg in the Conventwald. If Li uptake by plants significantly fractionates Li isotopes, the effect on the

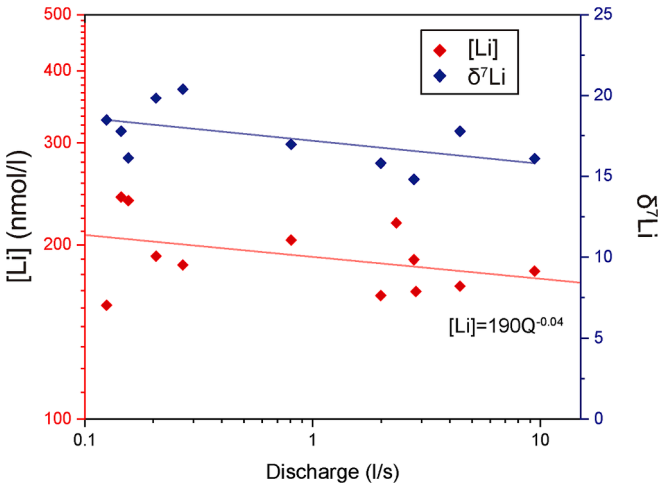

Fig. 8. Li concentrations ([Li]) and isotopic compositions (δ^{7}Li) of creek water samples in response to discharge variation.

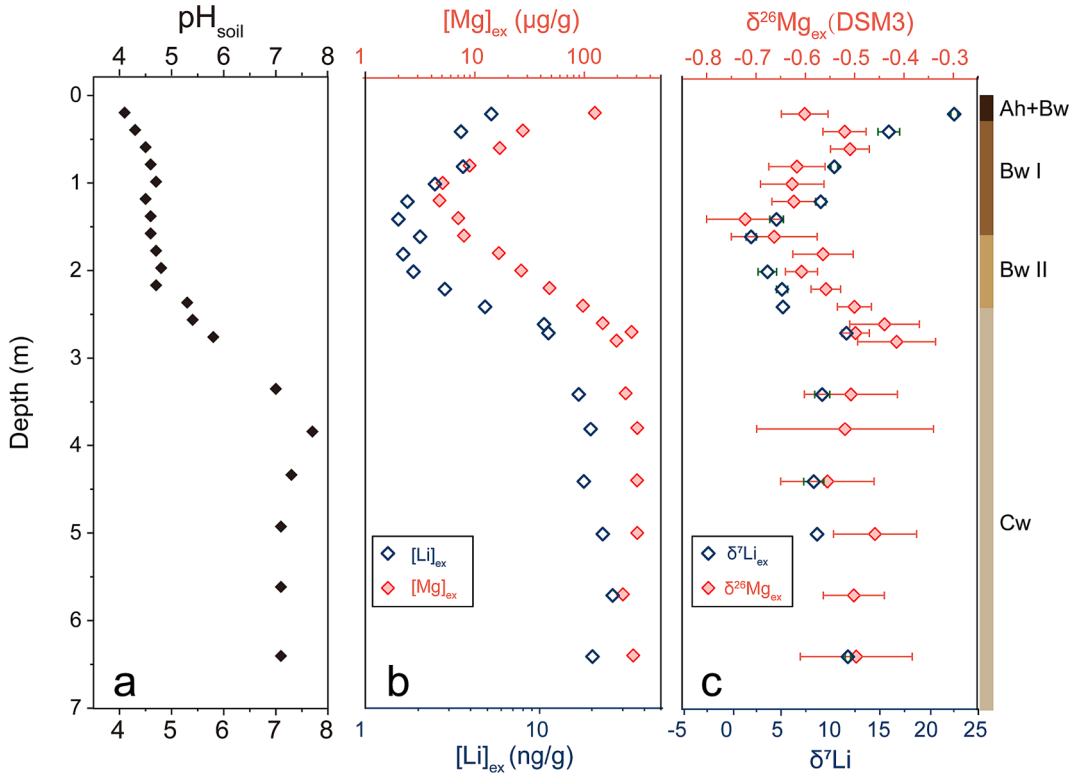

Fig. 9. Ph of the soil, concentrations and isotopic compositions of Li and Mg in the regolith exchangeable fraction (extracted by 1 M NH_4OAc). Uncertainty shown for the isotope ratios of the exchangeable fraction represents the twofold standard deviation of 3–4 replicate measurements. Analytical uncertainty for Li and Mg concentrations is better than 5 % based on repeated measurements of standard reference materials.

exchangeable fraction may be similarly high for the non-nutrient Li and the macronutrient Mg (Fig. 9). Unfortunately, our data is inadequate for a quantitative estimation of the plant-induced effect of isotope fractionation on the exchangeable fraction at the field scale because only twigs and leaves were measured in this study, meaning that the δ ^{7}Li value of the bulk tree remains unquantified. Nevertheless, future research focusing on Li isotope fractionation during biological cycling is encouraged as it is increasingly controversial as to whether Li isotopes are fractionated during plant uptake (Clergue et al., 2015; Gao et al., 2022; Lemarchand et al., 2010; Li et al., 2020).

5.4. A missing Li export path

Two of the observations presented above are striking. The first is that subsurface flow, groundwater, and creek water are all enriched in ^{7}Li, which means that water is continuously removing ^{7}Li in preference over ^{6}Li from regolith and eventually from the catchment. However, the regolith is isotopically indistinguishable from bedrock (Fig. 1), which is surprising as τ_{Li} shows that ~ 50 % of Li contained in parent rock was lost by weathering between 0 and 6 m depth (Fig. 5). The second is that the regolith weathering rate of Li ($W^{Li}_{regolith}$, 3.8 ± 0.3 × 10^{-3} g/m^2/y, Eq. 5) is much higher than the Li export flux found in the river dissolved load (W^{Li}_{river}, 0.9 ± 0.2 × 10^{-3} g/m^2/y, Eq. 6. Note, [Li] in unmeasured samples was extrapolated from [Li]-discharge relationship of measured samples, Fig. 8). Thus, there is an imbalance in fluxes. To explain these two observations, we expand upon watershed Li fluxes (Fig. 4) with an isotope-based budget.

At steady state, and integrating over the timescale of regolith formation the mass balance is (see Table 1 for definitions and Fig. 4 for flux estimates):

$$RP^{Li} = E^{Li}_{primaryminerals} + E^{Li}_{secondarysolids} + W^{Li}_{regolith} \quad (15)$$

To partition the total erosion rate of Li ($E^{Li}_{reglith}$) into the erosion rate of primary minerals and secondary minerals we derive the fraction of Li-bearing secondary minerals in regolith via an isotope-based end-member mixing equation (Eq. 11 in Table 1).

As the δ^7Li value of soil is almost identical to that of bedrock, calculated $f_{secondary}$ amounts to only 8 ± 6 %. This is a maximum estimation as we use the most positive δ^{7}Li value (-5.4 ‰) of our separated clay-sized fraction. A true secondary solid is expected to have a more negative δ^{7}Li value than the clay-size fraction (which may still contain some component of Li from primary minerals). Assuming steady state and that the fractionation is in equilibrium, $f_{secondary}$ can alternatively be calculated using Eq. 17:

$$f^{Li}_{\text{secondary}} = \frac{\delta^7 Li_{\text{rock}} - \delta^7 Li_{\text{diss}}}{\Delta^7 Li_{\text{secondary-diss}}} \times \tau_{Li} \quad (16)$$

Taking 18 ‰ as a representative apparent isotope fractionation factor for the formation of secondary minerals (Hindshaw et al., 2019; Vigier et al., 2008) and using the δ^{7}Li value of river water as δ^{7}Li$_{diss}$, this equation gives a $f_{secondary}$ of 48 ± 9 %, significantly higher than the value yielded by endmember mixing calculation (~8 ± 6 %, Eq. 11). In other words, while the isotope batch model (eq. 17) suggests that 48 % of the Li released by chemical weathering should be found in clays, only 8 % of this clay-bound Li is found in the regolith (eq. 11).

This apparent imbalance can also be evaluated from a flux perspective. We use the isotope model developed by Bouchez et al. (2013) to calculate the normalized dissolved Li export flux ($w^{Li}_{isotope}$, Eq. 10 in Table 1). Using δ^{7}Li values of regolith (δ^{7}Li$_{soil}$ = -1.7 ± 0.2 ‰), unweathered parent bedrock (δ^{7}Li$_{rock}$ = -1.5 ± 0.7 ‰), and creek water (δ^{7}Li$_{diss}$ ranges from 14.8 ± 0.1 to 20.4 ± 0.4 ‰), $w^{Li}_{isotope}$ amounts to 1.8 ± 1.5 % (2SD) to 2.4 ± 1.1 % (2SD), implying that Li is apparently almost entirely exported in particulate form, a conclusion contrary to

the normalized net solubilisation flux of Li ($w^{Li}_{regolith}$, Eq. 9 in Table 1) which amounts to 50 ± 12 %.

A similar discrepancy arises from a quantitative comparison of the dissolved Li export flux (W^{Li}_{river}) with the net solubilisation of Li from regolith ($W^{Li}_{regolith}$), where its ratio ($W^{Li}_{river}/W^{Li}_{regolith}$) is called the Li "dissolved export efficiency" (DEE^{Li}, Eq. 11 in Table 1, Uhlig et al., 2017, von Blanckenburg et al., 2021). In steady state and balanced fluxes, the DEE^{Li} value is defined to be 1, meaning the chemical weathering rate of Li inferred from water chemistry equals that inferred from Li depletion from regolith. However, at our site the calculated DEE^{Li} is 0.24 ± 0.08, suggesting that of Li solubilized from regolith, only ~ 24 % appears in the river dissolved load.

We note that DEE^{Li} is a ratio of fluxes that integrate over vastly different timescales: W^{Li}_{river} integrates over annual timescales but $W^{Li}_{regolith}$ over millennial timescales, over which climate and discharge may have fluctuated. To reduce a potentially introduced bias, we use a metric that is independent of timescale effects by normalizing W^{Li}_{river} and $W^{Li}_{regolith}$ over their respective Na fluxes (DEE^{Li}_{Na}, Eq.12, Uhlig et al., 2017), assuming the export of Na reflects congruent dissolution from rock and that Na behaves conservatively, i.e. that no Na is incorporated into secondary solids. An additional advantage of this approach is that unlike DEE^{Li}, DEE^{Li}_{Na} does not require knowledge of the individual fluxes.

Similar to DEE^{Li}, a DEE^{Li}_{Na} value of 1 means that dissolved Li export equals Li loss from the regolith, a value < 1 indicates that a fraction of Li lost from the regolith is missing in the river dissolved load export. At the Conventwald the DEE^{Li}_{Na} equals 0.30 ± 0.08 (Eq. 14 in Table 1, the variation is due to the [Li]/[Na] variation in river water), in agreement with the calculated DEE^{Li} (0.24 ± 0.08).

Two independent lines of evidence thus document the imbalance in the Li cycle at our study site: 1) the regolith's δ^7Li value is not negative enough to balance the ^{7}Li export by river water, and 2) Li in the riverine dissolved load only accounts for ~ 30 % of the Li solubilized from regolith. Therefore, a flux – or unsampled pool enriched in ^{6}Li – is not accounted for. von Blanckenburg et al., (2021) put forward four explanations for a potential imbalance in elemental fluxes based on their investigation into an "erodosequence": 1) methodological artefacts (for instance loss of colloidal material during filtration); 2) perturbation of steady state; 3) element fractionation along hillslopes or at depth; and 4) a hidden pathway or pool. Of these four, the authors conclude that the most likely is the latter "hidden pathway or pool". In support of this, other studies of catchment isotope cycling have identified imbalances in export pathways. For example, Uhlig et al., (2017) suggested that the removal of coarse woody debris might account for the unidentified export of heavy Mg isotopes. Similarly, Oeser and von Blanckenburg (2021) attributed the loss of ^{86}Sr to erosion of fractionated organic solids (i.e., leaf litter and woody debris). Biological uptake may also account for the imbalance in global K and Ba river export (Charbonnier et al., 2020; 2022).

For Li at our study site, a methodological artefact from loss of colloids during filtration is possible, but Wimpenny et al., (2010b) showed that the colloidal Li load is negligible compared to that in the truly dissolved phase. A 'hidden pathway' of erosion of plant debris, removal by logging, or accumulation in re-growing biomass cannot explain the discrepancy since Li is not a nutritive element and as such the Li flux into biological material should not be insufficient (Fig. 4). Moreover, our data suggest Li in plant tissues is enriched in ^{7}Li. Hence, its removal does not explain apparently missing ^{6}Li. However, removal of subsurface fine particles – with different chemical composition compared to bulk regolith – has been suggested as an alternative such hidden pathway that will deplete the regolith in particular elements and isotopes (Kim et al., 2018). Unbalanced budgets of B, Mg and Li isotopes have been attributed to this process (Noireaux et al., 2021; Steinhoefel et al., 2021; Ma et al., 2015). Here, we evaluate whether this potentially also explains the unbalanced Li flux at our study site. Although no sediments were sampled from river or seepage to constrain the chemistry of this fine particulate, our separated clay-sized fraction is the only compartment that exhibits more negative δ^7Li values than bedrock at this site. Assuming this fraction is representative of fine particulates that would be removed by subsurface flow, their export might present a viable hypothesis to explain the apparently unbalanced Li cycling. Given that this pathway remains unsampled, we can not assess whether it is sufficient to explain the ~ 40 % discrepancy between expected $f_{secondary}$ based on an isotope mass balance (Eq. 17; 48 ± 9 %), and that derived from an endmember mixing calculation in the regolith (8 ± 6 %). Similarly, whether this unidentified flux could also explain the discrepancy between $W^{Li}_{regolith}$ (2.8 ± 0.3 mg/m^2/y, calculated using τ^{Li}_{Zr}, bedrock concentration, and denudation rate) and W^{Li}_{river} (0.9 ± 0.2 mg/m^2/y, calculated using river water chemistry and discharge) needs evaluation.

In sum, then, export of fine particulates via subsurface flow is a promising candidate for the "hidden export pathway" that explains the imbalances in isotope budgets and chemical weathering fluxes observed at our study site. Further work considering comprehensive sampling of river/seepage sediments (Gu et al., 2021; Kim et al., 2018) along with identification and quantitative separation of its origin (from surface erosion and subsurface export) is, however, required to evaluate this hypothesis, as is the search for fine particles such as those found in sedimentary sink areas (Ma et al., 2016 and Zhang et al., 2023). Given that such discrepancies are an increasingly common observation in Critical Zone research, such detailed investigations seem warranted.

6. Conclusions

We observed that in a temperate forested catchment the separated clay-sized fraction of the regolith exhibits more negative δ^7Li values than the bulk regolith. This secondary solid formation in turn drives the δ^7Li value of the regolith exchangeable fraction and of the dissolved fluid to more positive values. Water may, however, be impacted by different geological processes at different depths and thus exhibit different evolution pathways on its δ^7Li value. Conservative mixing, exchangeable pool buffering, and Li incorporation or adsorption are direct processes controlling the δ^7Li value of subsurface flow, groundwater and river water, respectively. The subsurface structure of the Critical Zone thus presents a crucial factor when considering the isotope labels disclosed by water chemistry. Nevertheless, although causal drivers of δ^7Li variability between discrete water samples may vary, in each case secondary mineral formation is the primary process responsible for δ^7Li fractionation. At this study site Li cycling is not balanced, given that the δ^7Li value of regolith is not negative enough to balance the isotopically heavy Li exported by river water, and given that Li in the river dissolved load only accounts for 30 ± 8 % of Li solubilized from regolith. These discrepancies might be reconciled by the existence of a hidden export pathway through removal in subsurface flow of fine particulates that have lower δ^7Li values than the bulk regolith. While such imbalances have been noted in studies of the nutritive elements K and Ba in big rivers, suggesting an undisclosed biogenic pathway, they are absent for Li and Na in big rivers (Charbonnier et al., 2022). One potential explanation for the absence of such imbalance in large rivers is a scale effect: while at the hillslope scale fluxes are subject to large heterogeneity introduced by the belowground structure in the Critical Zone, these fluxes and their isotopes average out once solutes have emerged in large river dissolved and sedimentary loads. Nevertheless, since observations of isotopic and flux imbalance in the Critical Zone are increasingly reported, this hidden export pathway merits further investigation.

CRediT authorship contribution statement

Di Cai: Conceptualization, Data curation, Formal analysis, Investigation, Methodology, Visualization, Writing – original draft, Writing –

review & editing. **Michael J. Henehan:** Conceptualization, Formal analysis, Investigation, Supervision, Validation, Writing – original draft, Writing – review & editing. **David Uhlig:** Formal analysis, Investigation, Methodology, Project administration, Validation, Writing – original draft, Writing – review & editing. **Friedhelm von Blanckenburg:** Conceptualization, Formal analysis, Funding acquisition, Investigation, Project administration, Supervision, Validation, Writing – original draft, Writing – review & editing.

Declaration of competing interest

The authors declare that they have no known competing financial interests or personal relationships that could have appeared to influence the work reported in this paper.

Data availability

Research Data associated with this article can be accessed at GFZ Data Services under the reference Cai et al. (2021). https://doi.org/10.5880/GFZ.3.3.2021.005.

Acknowledgements

The authors are grateful for funding from the German National Science Foundation Priority Program 1685 “Ecosystem nutrition: forest strategies for limited phosphorus resources” and to Friederike Lang for coordination. Di Cai is grateful for funding by a CSC scholarship. Johannes Glodny is acknowledged for support on mineral separation. The authors are grateful to the analytical support provided by Jutta Schlegel and Josefine Holtz. We thank the careful reviews by Quentin Charbonnier and two anonymous reviewers. The authors also acknowledge the valuable contributions of Associate Editor Jiubin Chen and Executive Editor Jeffrey Catalano for their handling of the manuscript and insightful comments.

References

Bachmair, S., Weiler, M., 2012. Technical report on experimental hillslope hydrology. University of Freiburg, Freiburg, Germany, Hydronotes.
Bouchez, J., von Blanckenburg, F., Schuessler, J.A., 2013. Modeling novel stable isotope ratios in the weathering zone. Am. J. Sci. 313, 267–308.
Brantley, S.L., Goldhaber, M.B., Ragnarsdottir, K.V., 2007. Crossing disciplines and scales to understand the critical zone. Elements 3, 307–314.
Brimhall, G.H., Dietrich, W.E., 1987. Constitutive mass balance relations between chemical composition, volume, density, porosity, and strain in metasomatic hydrochemical systems: Results on weathering and pedogenesis. Geochim. Cosmochim. Acta 51, 567–587.
Bullen, T., Chadwick, O., 2016. Ca, Sr and Ba stable isotopes reveal the fate of soil nutrients along a tropical climosequence in Hawaii. Chem. Geol. 422, 25–45.
Cai, D; Henehan, M.J.; von Blanckenburg, F., Uhlig, D. 2021. Dataset on Biogeochemical cycling of Mg and Li isotopes in the Conventwald (the Black Forest, Germany). GFZ Data Services. doi: 10.5880/GFZ.3.3.2021.005.
Cai, D., Henehan, M.J., Uhlig, D., von Blanckenburg, F., 2022. Mg isotope composition of runoff is buffered by the regolith exchangeable pool. Geochim. Cosmochim. Acta 321, 99–114.
Chapela Lara, M., Buss, H.L., Henehan, M.J., Schuessler, J.A., McDowell, W.H., 2022. Secondary minerals drive extreme lithium isotope fractionation during tropical weathering. J. Geophys. Res. Earth Surf. 127.
Charbonnier, Q., Bouchez, J., Gaillardet, J., Gayer, É., 2020. Barium stable isotopes as a fingerprint of biological cycling in the Amazon River basin. Biogeosciences 17, 5989–6015.
Charbonnier, Q., Bouchez, J., Gaillardet, J., Gayer, E., Porder, S., 2022. A global imbalance in potassium and barium river export: the result of biological uptake? Geochem. Perspect. Lett. 21, 32–36.
Clergue, C., Dellinger, M., Buss, H.L., Gaillardet, J., Benedetti, M.F., Dessert, C., 2015. Influence of atmospheric deposits and secondary minerals on Li isotopes budget in a highly weathered catchment, Guadeloupe (lesser Antilles). Chem. Geol. 414, 28–41.
Dellinger, M., Gaillardet, J., Bouchez, J., Calmels, D., Louvat, P., Dosseto, A., Gorge, C., Alanoca, L., Maurice, L., 2015. Riverine Li isotope fractionation in the Amazon River basin controlled by the weathering regimes. Geochim. Cosmochim. Acta 164, 71–93.
Gaillardet, J., Dupré, B., Allègre, C.J., 1999. Geochemistry of large river suspended sediments: silicate weathering or recycling tracer? Geochim. Cosmochim. Acta 63, 4037–4051.
Gao, J., Yu, Y., Wang, D., Wang, W., Yu, F., Zhang, S., Wang, C., Dai, H., Hao, X., Cen, K., 2022. Multielement biogeochemistry and lithium isotopic composition of the dominant plants at the Jiajika mine, western Sichuan, China – The largest hard rock-type lithium mine in Asia. Appl. Geochem. 136, 105138.
Gislason, S., Arnorsson, S., Ármannsson, H., 1996. Chemical weathering of basalt in Southwest Iceland: Effects of runoff, age of rocks and vegetative/glacial cover. Am. J. Sci. 296, 837–907.
Gottselig, N., Sohrt, J., Uhlig, D., Nischwitz, V., Weiler, M., Amelung, W., 2020. Groundwater controls on colloidal transport in forest stream waters. Sci. Total Environ. 717, 134638.
Gou, L.-F., Jin, Z., Pogge von Strandmann, P.A.E., Li, G., Qu, Y.-X., Xiao, J., Deng, L., Galy, A., 2019. Li isotopes in the middle Yellow River: Seasonal variability, sources and fractionation. Geochim. Cosmochim. Acta 248, 88–108.
Gu, X., Kim, H., Hynek, S., Thompson, A., Brantley, S.L., 2021. Subsurface particle transport shapes the deep critical zone in a granitoid watershed. Geochem. Perspect. Lett. 13–18.
Henchiri, S., Gaillardet, J., Dellinger, M., Bouchez, J., Spencer, R.G.M., 2016. Riverine dissolved lithium isotopic signatures in low-relief Central Africa and their link to weathering regimes. Geophys. Res. Lett. 43, 4391–4399.
Hindshaw, R.S., Tosca, R., Tosca, N.J., Tipper, E.T., 2019. Experimental constraints on Mg isotope fractionation during clay formation: Implications for the global biogeochemical cycle of Mg. Earth Planet. Sci. Lett., 115980
Hoefs, J., 2021. Stable isotope geochemistry, springer textbooks in earth sciences, geography and environment. Springer International Publishing, Cham.
Huh, Y., Chan, L.-H., Zhang, L., Edmond, J.M., 1998. Lithium and its isotopes in major world rivers: implications for weathering and the oceanic budget. Geochim. Cosmochim. Acta 62, 2039–2051.
Huh, Y., Chan, L.-H., Edmond, J.M., 2001. Lithium isotopes as a probe of weathering processes: Orinoco River. Earth Planet. Sci. Lett. 194, 189–199.
Kim, H., Bishop, J.K.B., Dietrich, W.E., Fung, I.Y., 2014. Process dominance shift in solute chemistry as revealed by long-term high-frequency water chemistry observations of groundwater flowing through weathered argillite underlying a steep forested hillslope. Geochim. Cosmochim. Acta 140, 1–19.
Kim, H., Gu, X., Brantley, S.L., 2018. Particle fluxes in groundwater change subsurface shale rock chemistry over geologic time. Earth Planet. Sci. Lett. 500, 180–191.
Kısakűrek, B., James, R.H., Harris, N.B.W., 2005. Li and δ7Li in Himalayan rivers: Proxies for silicate weathering? Earth planet. Sci. Lett. 237, 387–401.
Lang, F., Krüger, J., Amelung, W., Willbold, S., Frossard, E., Bünemann, E.K., Bauhus, J., Nitschke, R., Kandeler, E., Marhan, S., Schulz, S., Bergkemper, F., Schloter, M., Luster, J., Guggisberg, F., Kaiser, K., Mikutta, R., Guggenberger, G., Polle, A., Pena, R., Prietzel, J., Rodionov, A., Talkner, U., Meesenburg, H., von Wilpert, K., Hölscher, A., Dietrich, H.P., Chmara, I., 2017. Soil phosphorus supply controls P nutrition strategies of beech forest ecosystems in Central Europe. Biogeochemistry 136, 5–29.
Lemarchand, E., Chabaux, F., Vigier, N., Millot, R., Pierret, M.-C., 2010. Lithium isotope systematics in a forested granitic catchment (Strengbach, Vosges Mountains, France). Geochim. Cosmochim. Acta 74, 4612–4628.
Li, W., Liu, X.-M., Chadwick, O.A., 2020. Lithium isotope behavior in Hawaiian regoliths: Soil-atmosphere-biosphere exchanges. Geochim. Cosmochim. Acta 285, 175–192.
Li, W., Liu, X.-M., 2020. Experimental investigation of lithium isotope fractionation during kaolinite adsorption: Implications for chemical weathering. Geochim. Cosmochim. Acta 284, 156–172.
Li, W., Liu, X.-M., 2022. Mineralogy and fluid chemistry controls on lithium isotope fractionation during clay adsorption. Sci. Total Environ. 851, 158138.
Li, W., Liu, X.-M., Wang, K., Koefoed, P., 2021. Lithium and potassium isotope fractionation during silicate rock dissolution: An experimental approach. Chem. Geol. 568, 120142.
Liu, X.-M., Rudnick, R.L., McDonough, W.F., Cummings, M.L., 2013. Influence of chemical weathering on the composition of the continental crust: Insights from Li and Nd isotopes in bauxite profiles developed on Columbia River basalts. Geochim. Cosmochim. Acta 115, 73–91.
Liu, X.-M., Wanner, C., Rudnick, R.L., McDonough, W.F., 2015. Processes controlling δ7Li in rivers illuminated by study of streams and groundwaters draining basalts. Earth Planet. Sci. Lett. 409, 212–224.
Ma, L., Teng, F.-Z., Jin, L., Ke, S., Yang, W., Gu, H.-O., Brantley, S.L., 2015. Magnesium isotope fractionation during shale weathering in the Shale Hills critical zone observatory: Accumulation of light Mg isotopes in soils by clay mineral transformation. Chem. Geol. 397, 37–50.
Maher, K., 2010. The dependence of chemical weathering rates on fluid residence time. Earth Planet. Sci. Lett. 294, 101–110.
Maher, K., 2011. The role of fluid residence time and topographic scales in determining chemical fluxes from landscapes. Earth Planet. Sci. Lett. 312, 48–58.
Millot, R., Vigier, N., Gaillardet, J., 2010. Behaviour of lithium and its isotopes during weathering in the Mackenzie Basin. Canada. Geochim. Cosmochim. Acta 74, 3897–3912.
Misra, S., Froelich, P.N., 2012. Lithium isotope history of cenozoic seawater: Changes in silicate weathering and reverse weathering. Science 335, 818–823.
Noireaux, J., Sullivan, P.L., Gaillardet, J., Louvat, P., Steinhoefel, G., Brantley, S.L., 2021. Developing boron isotopes to elucidate shale weathering in the critical zone. Chem. Geol. 559, 119900.
Oeser, R.A., von Blanckenburg, F., 2020. Strontium isotopes trace biological activity in the critical zone along a climate and vegetation gradient. Chem. Geol. 558, 119861.
Penniston-Dorland, S., Liu, X.-M., Rudnick, R.L., 2017. Lithium isotope geochemistry. Rev. Mineral. Geochem. 82, 165–217.
Pistiner, J.S., Henderson, G.M., 2003. Lithium-isotope fractionation during continental weathering processes. Earth Planet. Sci. Lett. 214, 327–339.

Pogge von Strandmann, P.A.E., Burton, K.W., James, R.H., van Calsteren, P., Gíslason, S. R., Mokadem, F., 2006. Riverine behaviour of uranium and lithium isotopes in an actively glaciated basaltic terrain. Earth Planet. Sci. Lett. 251, 134–147.
Pogge von Strandmann, P.A.E., Henderson, G.M., 2015. The Li isotope response to mountain uplift. Geology 43, 67–70.
Pogge von Strandmann, P.A.E.P., Kasemann, S.A., Wimpenny, J.B., 2020. Lithium and lithium isotopes in earth's surface cycles. Elements 16, 253–258.
Pogge von Strandmann, P.A.E., Opfergelt, S., Lai, Y.-J., Sigfússon, B., Gislason, S.R., Burton, K.W., 2012. Lithium, magnesium and silicon isotope behaviour accompanying weathering in a basaltic soil and pore water profile in Iceland. Earth Planet. Sci. Lett. 339–340, 11–23.
Pogge von Strandmann, P.A.E., Frings, P.J., Murphy, M.J., 2017. Lithium isotope behaviour during weathering in the Ganges alluvial plain. Geochim. Cosmochim. Acta 198, 17–31.
Pogge von Strandmann, P.A.E., Fraser, W.T., Hammond, S.J., Tarbuck, G., Wood, I.G., Oelkers, E.H., Murphy, M.J., 2019. Experimental determination of Li isotope behaviour during basalt weathering. Chem. Geol. 517, 34–43.
Pogge von Strandmann, P.A.E., Burton, K.W., Opfergelt, S., Genson, B., Guicharnaud, R. A., Gislason, S.R., 2021. The lithium isotope response to the variable weathering of soils in Iceland. Geochim. Cosmochim. Acta 313, 55–73.
Poppe, L.J., Paskevich, V.F., Hathaway, J.C., Blackwood, D.S., 2001. A laboratory manual for X-ray powder diffraction. US Geological Survey Open-File Report 1 (041), 1–88.
Qi, H.P., Taylor, P.D.P., Berglund, M., De Bièvre, P., 1997. Calibrated measurements of the isotopic composition and atomic weight of the natural Li isotopic reference material IRMM-016. Int. J. Mass Spectrom. Ion Process. 171, 263–268.
Ryu, J.-S., Vigier, N., Lee, S.-W., Lee, K.-S., Chadwick, O.A., 2014. Variation of lithium isotope geochemistry during basalt weathering and secondary mineral transformations in Hawaii. Geochim. Cosmochim. Acta 145, 103–115.
Sohrt, J., Uhlig, D., Kaiser, K., von Blanckenburg, F., Siemens, J., Seeger, S., Frick, D.A., Krüger, J., Lang, F., Weiler, M., 2019. Phosphorus fluxes in a temperate forested watershed: Canopy leaching, runoff sources, and in-stream transformation. Front. for. Glob. Change 2, 85.
Steinhoefel, G., Brantley, S.L., Fantle, M.S., 2021. Lithium isotopic fractionation during weathering and erosion of shale. Geochim. Cosmochim. Acta 295, 155–177.
Sullivan, P.L., Ma, L., West, N., Jin, L., Karwan, D.L., Noireaux, J., Steinhoefel, G., Gaines, K.P., Eissenstat, D.M., Gaillardet, J., Derry, L.A., Meek, K., Hynek, S., Brantley, S.L., 2016. CZ-tope at Susquehanna Shale Hills CZO: Synthesizing multiple isotope proxies to elucidate critical zone processes across timescales in a temperate forested landscape. Chem. Geol. 445, 103–119.
Tipper, E.T., Stevenson, E.I., Alcock, V., Knight, A.C.G., Baronas, J.J., Hilton, R.G., Bickle, M.J., Larkin, C.S., Feng, L., Relph, K.E., Hughes, G., 2021. Global silicate weathering flux overestimated because of sediment–water cation exchange. Proc. Natl. Acad. Sci. 118.
Tomascak, P.B., Magna, T., Dohmen, R., 2016. Advances in lithium isotope geochemistry, advances in isotope geochemistry. Springer International Publishing, Cham.
Turton, D.J., Haan, C.T., Miller, E.L., 1992. Subsurface flow responses of a small forested catchment in the Ouachita mountains. Hydrol. Process. 6, 111–125.
Uhlig, D., Schuessler, J.A., Bouchez, J., Dixon, J.L., von Blanckenburg, F., 2017. Quantifying nutrient uptake as driver of rock weathering in forest ecosystems by magnesium stable isotopes. Biogeosciences 14, 3111–3128.
Uhlig, D., Amelung, W., von Blanckenburg, F., 2020. Mineral nutrients sourced in deep regolith sustain long-term nutrition of mountainous temperate Forest ecosystems. Glob. Biogeochem. Cycles 34, e2019GB006513.
Uhlig, D., & von Blanckenburg, F. 2019b. Geochemical and isotope data on rock weathering, and nutrient balances during fast forest floor turnover in montane, temperate forest ecosystems. GFZ Data Services. doi: 10.5880/GFZ.3.3.2019.004.
Uhlig, D., von Blanckenburg, F., 2019a. How slow rock weathering balances nutrient loss during fast Forest floor turnover in montane, temperate forest ecosystems. Front. Earth Sci. 7.
Vigier, N., Decarreau, A., Millot, R., Carignan, J., Petit, S., France-Lanord, C., 2008. Quantifying li isotope fractionation during smectite formation and implications for the li cycle. Geochim. Cosmochim. Acta 72, 780–792.
Vigier, N., Gislason, S.R., Burton, K.W., Millot, R., Mokadem, F., 2009. The relationship between riverine lithium isotope composition and silicate weathering rates in Iceland. Earth Planet. Sci. Lett. 287, 434–441.
von Blanckenburg, F., Schuessler, J.A., Bouchez, J., Frings, P.J., Uhlig, D., Oelze, M., Frick, D.A., Hewawasam, T., Dixon, J., Norton, K., 2021. Rock weathering and nutrient cycling along an erodosequence. Am. J. Sci. 321, 1111–1163.
Wang, Q.-L., Chetelat, B., Zhao, Z.-Q., Ding, H., Li, S.-L., Wang, B.-L., Li, J., Liu, X.-L., 2015. Behavior of lithium isotopes in the Changjiang River system: Sources effects and response to weathering and erosion. Geochim. Cosmochim. Acta 151, 117–132.
Wanner, C., Sonnenthal, E.L., Liu, X.-M., 2014. Seawater δ7Li: A direct proxy for global CO2 consumption by continental silicate weathering? Chem. Geol. 381, 154–167.
Wimpenny, J., Gíslason, S.R., James, R.H., Gannoun, A., Pogge Von Strandmann, P.A.E., Burton, K.W., 2010a. The behaviour of li and mg isotopes during primary phase dissolution and secondary mineral formation in basalt. Geochim. Cosmochim. Acta 74, 5259–5279.
Wimpenny, J., James, R.H., Burton, K.W., Gannoun, A., Mokadem, F., Gíslason, S.R., 2010b. Glacial effects on weathering processes: New insights from the elemental and lithium isotopic composition of West Greenland rivers. Earth Planet. Sci. Lett. 290, 427–437.
Wimpenny, J., Colla, C.A., Yu, P., Yin, Q.-Z., Rustad, J.R., Casey, W.H., 2015. Lithium isotope fractionation during uptake by gibbsite. Geochim. Cosmochim. Acta 168, 133–150.
WRB, I.W.G., 2014. World Reference Base for Soil Resources 2014. International Soil Classification System For Naming Soils And Creating Legends For Soil Maps. World Soil Resources Report No. 106. FAO, Rome.
Zhang, F., Dellinger, M., Hilton, R.G., Yu, J., Allen, M.B., Densmore, A.L., Sun, H., Jin, Z., 2022. Hydrological control of river and seawater lithium isotopes. Nat. Commun. 13, 3359.
Zhang, X. (Yvon), Saldi, G.D., Schott, J., Bouchez, J., Kuessner, M., Montouillout, V., Henehan, M., Gaillardet, J., 2021. Experimental constraints on Li isotope fractionation during the interaction between kaolinite and seawater. Geochim. Cosmochim. Acta 292, 333–347.
Zhang, X. (Yvon), Bajard, M., Bouchez, J., Sabatier, P., Poulenard, J., Arnaud, F., Crouzet, C., Kuessner, M., Dellinger, M., Gaillardet, J., 2023. Evolution of the alpine Critical Zone since the Last Glacial Period using Li isotopes from lake sediments. Earth Planet. Sci. Lett. 624, 118463.
Zhang, J.-W., Zhao, Z.-Q., Yan, Y.-N., Cui, L.-F., Wang, Q.-L., Meng, J.-L., Li, X.-D., Liu, C.-Q., 2021. Lithium and its isotopes behavior during incipient weathering of granite in the eastern tibetan plateau. China. Chem. Geol. 559, 119969.
Zhao, P., Tang, X., Zhao, P., Wang, C., Tang, J., 2013. Identifying the water source for subsurface flow with deuterium and oxygen-18 isotopes of soil water collected from tension lysimeters and cores. J. Hydrol. 503, 1–10.
Zhu, G., Ma, J., Wei, G., Zhang, L., Wang, Z., Zhang, Z., Zeng, T., 2023. Lithium isotope fractionation during the weathering of granite: Responses to pH. Geochim. Cosmochim. Acta 345, 117–129.